Supporting Information

Tuning the Interfacial Chemistry in Metal Organic Framework/Graphene Electrodes for Boosting Energy Storage

Shashank Sundriyal[1*], Vishal Shrivastav[1], Prashant Dubey[2], Mansi[1], Vit Kvasnička[1,3], Mahima Khandelwal[1], Aby Cheruvathoor Poulose[1], Radek Zbořil[1,3*], Aristides Bakandritsos[1,3*]

[1]Regional Center of Advanced Technologies and Materials, The Czech Advanced Technology and Research Institute (CATRIN), Palacký University Olomouc, Šlechtitelů 27, 779 00 Olomouc, Czech Republic;

[2]Advanced Carbon Products and Metrology Department, CSIR-National Physical Laboratory (CSIR-NPL), New Delhi 110012, India;

[3]Nanotechnology Centre, Centre for Energy and Environmental Technologies, VŠB–Technical University of Ostrava, 17. listopadu 2172/15, 708 00 Ostrava-Poruba, Czech Republic;

***Correspondence:** shashank.sundriyal@upol.cz (Dr. Shashank Sundriyal), a.bakandritsos@upol.cz (Dr. Aristides Bakandritsos), radek.zboril@upol.cz (Prof. Radek Zboril)

1. EXPERIMENTAL SECTION

1.1 Materials

Graphite Fluoride (>61 wt. % F), NaCN (≤15.0 ppm Trace Metal Analysis), ethylene glycol (anhydrous, 99.8%), poly(vinylidene fluoride), N-methyl-2- pyrrolidone (anhydrous, 99.5%), were purchased from Sigma-Aldrich. Acetone (min. 99.0 %), ethanol (absolute, >96%), and Sulfuric acid (96%) were purchased from Penta. Nickel acetate tetrahydrate (>95.0%), 2,3,6,7,10,11-hexahydroxytriphenylene (HHTP) (>95%) was purchased from TCI, Europe. Active carbon (type YP-80F) was obtained from Kuraray. Amine-free N,N-dimethylformamide (DMF) (min. 98 %), and nitric acid (Analupure®, 65%) were obtained from Lach-Ner. All reagents were used without further purification. Ultrapure water was obtained from Mirae ST Instrument (Esse-

UP Analysis, S00005812). Graphite foil (99.85% C; Thickness: 0.2 mm) is procured from ProGraphite Germany.

1.2 Methods

1.2.1 Synthesis of graphene acid (GA)

The graphene acid was prepared according to our previous reports.[1] Briefly, the commercial graphite fluoride (120 mg) is placed in a 25 mL round bottom glass flask with 15 mL of DMF and sonicated for 4h under a nitrogen atmosphere. Subsequently, 800 mg NaCN was added and the mixture was heated at 130 °C with a condenser under stirring (500 rpm) for 24 h. The mixture was left to cool to room temperature, and an equal amount of acetone was added. The materials were then separated by centrifugation and further purified by successive washing steps using DMF, dichloromethane, acetone, ethanol, and water (all 4×). Afterward, the material was washed with hot (80 °C) DMF and water. During the final centrifugation with water, it was necessary to apply centrifugal forces of up to 25000 rpm to isolate the product cyanographene. The cyanographene was transformed into graphene acid by mixing it with HNO_3 (65%) under stirring at room temperature. Afterward, the mixture was then heated at 100 °C and stirred (350 rpm) for 24 h. The final product was thoroughly washed with water to remove soluble impurities and then freeze-dried to obtain a powder.

1.2.2 Synthesis of 2D $Ni_3(HHTP)_2$ (2DNi)

The 2DNi CMOF was synthesized as per the previous literature report with some modifications.[2] To synthesize 2DNi CMOF, 140 mg of HHTP and 200 mg of Nickel acetate tetrahydrate were dissolved in 80 mL deionized water in a 200 mL reagent glass bottle. The bottle was stirred for 45 minutes until the dispersion was prepared uniformly. After that, the reaction mixture was heated

in an isothermal oven at 85 ℃ for 18 hrs. The reaction mixture was cooled to room temperature and subsequently washed with DI water and acetone (4× each) respectively, and finally dried overnight at 70 ℃ and then ground to form a powder.

1.2.3 Synthesis of 2D $Ni_3(HHTP)_2$/graphene acid composite (2DNiGA)

For the synthesis of 2DNiGA composite, firstly 120 mg graphene acid is dissolved in 80 mL DI water (1.5 mg mL^{-1}) via ultrasonication for 1 hour in a 200 mL reagent glass bottle. After that 140 mg of HHTP and 200 mg of Nickel acetate tetrahydrate are mixed into the GA dispersion and stirred for 45 minutes to prepare the uniform mixture. After that, the reaction mixture was heated in an isothermal oven at 85 ℃ for 18 hrs. The reaction mixture was cooled to room temperature and subsequently washed with DI water and acetone (4× each) respectively and finally dried overnight at 70 ℃ and then ground to form a powder.

1.3 Material Characterization

The successful formation of GA, 2DNi, and 2DNiGA samples has been evaluated using different characterization techniques. X-ray diffraction (XRD) was recorded with an X'Pert PRO MPD (PANalytical) diffractometer in the Bragg–Brentano geometry, Co-Kα radiation (40 kV, 30 mA, 0.1789 nm) equipped with an X'Celerator detector and programmable divergence and diffracted beam anti-scatter slits. Infra-red spectra were measured on an iS5 FTIR spectrometer (Thermo Nicolet), with ZnSe crystal. A drop of a dispersion of the sample in ethanol or water was placed on a ZnSe crystal and left to dry and form a film in at ambient environment. Raman spectra were obtained on a DXR Raman microscope, the 633 nm excitation line diode laser was used. X-ray photoelectron spectroscopy (XPS) was carried out with the Nexsa G2 Surface Analysis System (Thermo Scientific™) spectrometer using an Al Kα source (15 kV, 50 W, spot size 100 μm). The

prepared samples were dispersed in acetone beforehand and then deposited onto a pure silicon wafer to be analyzed once dried. All binding energies were referenced to the C1s core level of the C-C bond set to the nominal value of 284.8 eV. The obtained data were evaluated and deconvoluted with the MultiPak (Ulvac-PHI, Inc.) software package. The morphology was characterized through scanning electron microscopy using a Hitachi SU6600 instrument with an accelerating voltage of 5 kV and transmission electron microscopy was obtained with a JEOL 2100 TEM, equipped with an emission gun of LaB_6 type, operating at 160 kV. High-resolution transmission electron microscopy (HR-TEM) in high-angle annular dark-field (HAADF) mode for elemental mapping were performed with an FEI TITAN G2 60-300 HRTEM microscope with an X-FEG type emission gun, operating at 300 kV, objective-lens image spherical aberration corrector, and ChemiSTEM energy-dispersive X-ray spectroscopy (EDS) detector. Thermal analyses were performed in open α-Al_2O_3 crucibles with a Netzsch STA 449C Jupiter instrument with an adapted quadrupole mass spectrometer (QMS 403C Aëolos) at a heating rate of 10 °C min^{-1}, under a nitrogen flow in the sample compartment.

1.4 Electrode Preparation and Electrochemical Characterization

The first step involves the preparation of the working electrode by forming a uniform slurry. For the slurry preparation, active material (2DNi, GA, and 2DNiGA) was mixed with Kuraray Carbon (YP-80F), and PVDF binder in an 8:1:1 w/w ratio respectively in NMP solvent uniformly. The obtained slurry thus produced was drop cast over graphite foil (current collector) with a specific dimension (1 x 1 cm^2) and then dried in a vacuum oven for 12h at 70°C, resulting in the working electrode with mass loading of ~1 mg cm^{-2}. The preliminary electrochemical analysis was done in a three-electrode configuration utilizing platinum as a counter, Ag/AgCl as a reference, and the as-prepared electrode as a working electrode. The electrochemical performance of the electrodes

was assessed using a VSP300 potentiostat/galvanostat (Bio-Logic) instrument at room temperature. Electrochemical impedance spectroscopy (EIS) was done in the 10 mHz to 100 KHz frequency range with 10 mV of voltage amplitude. Cyclic voltammetry (CV) was measured at varying scan rates from 5 to 100 mV s^{-1} while Galvanostatic charge-discharge (GCD) measurements were performed at different current densities from 0.5 to 10 A g^{-1}. All the electrochemical measurements were performed within a potential window of 0 to 1 V using 1M H_2SO_4 electrolyte.

In a two-electrode system, a hybrid supercapacitor (HSC) device is assembled using 2DNiGA as the positive electrode and GA as the negative electrode by performing proper mass balancing. The optimized potential window of the device is 1.6 V. For HSC assembling, the positive and negative electrode and filter paper (with pores 0.45 μm in size) were soaked in 1M H_2SO_4 electrolyte. After that, the separator was then sandwiched between both electrodes and sealed with paraffin film to avoid any leakage of electrolyte. Finally, the as-fabricated HSC device is tested in a two-electrode configuration to determine its cyclic stability, specific capacitance, energy density, and power density.

1.5 Calculations of Electrochemical Parameters

(A) Using a three-electrode system

(i) Specific capacitance using cyclic voltammetry (CV) curves was calculated using the following equation:

$$C_s = \frac{1}{ms(\Delta V)}\int IdV \qquad \text{(S1)}$$

where (∫IdV) = integral area of reduction part of CV curve, m = mass of active material on the electrode in g, ΔV = potential window, C_s= specific capacitance in F g^{-1}, and s = scan rate in V s^{-1}.

The galvanostatic charge–discharge (GCD) plots were used to calculate various parameters as mentioned under curves calculations:

(ii) Specific capacitance:

$$C_s = \frac{2I\int V dt}{\Delta V^2 \times m} \quad \text{(S2)}$$

where I = discharge current, m = mass of active materials on the electrode in g, ∫Vdt = Integral of the non-linear discharge part of GCD plot, and ΔV = potential window.

(iii) Electrochemical Surface Area (ECSA) Calculation:

To determine the electrochemical surface area (ECSA), cyclic voltammograms were measured at different scan rates (2 to 12 mV s^{-1}) between 0.6-0.8 V vs. Ag/AgCl. The electrochemical double layer capacitance (C_{EDLC}) was calculated using the following equation:

$$i_c = \nu \times C_{EDLC} \quad \text{(S3)}$$

where i_c is the capacitive cathodic/anodic current (mA), and ν is the scan rate (mV s^{-1}). Assuming that the capacitance obtained between 0.6–0.8 V is the EDLC, the slope of i_c–ν plot should be equal to C_{EDLC}. Thus, the ECSA can be calculated as follows:

$$\text{ECSA} = \frac{C_{EDLC}}{C^*} \quad \text{(S4)}$$

where the value of the general specific capacitance (C*) is 35 μF cm^{-2} in 1 M H_2SO_4

(B) Using a hybrid supercapacitor (two-electrode system)

For asymmetric supercapacitor fabrication, the charge balancing is required and will follow the relationship $q_+ = q_-$. The charge stored by each electrode depends on their respective mass (m), potential difference (V), and specific capacitance (C) following the below Eq.:

$$q_+ = C_+ \Delta V_+ m_+ \quad \text{(S5)}$$

and to get $q_+ = q_-$, the mass balancing will be done with the following equation:

$$C_+ \Delta V_+ m_+ = C_- \Delta V_- m_- \quad \text{(S6)}$$

From the mass balancing, the mass ratio of m(GA)/m(2DNiGA) was evaluated to be 2:1.

GCD based studies were used to calculate various parameters as elaborated by the following equations:

Gravimetric Capacitance-

$$C_g = \frac{I \times \Delta t}{\Delta V \times m_t} \quad \text{(S7)}$$

Areal Capacitance-

$$C_A = \frac{I \times \Delta t}{\Delta V \times A} \quad \text{(S8)}$$

Volumetric Capacitance-

$$C_V = C_g \times \rho \quad \text{(S9)}$$

Gravimetric energy and power density in W h kg^{-1} and W kg^{-1} respectively

$$\mathrm{Eg} = \frac{1 \times C_g \times (\Delta V^2)}{2 \times 3.6} \quad \text{(S10)}$$

$$\mathrm{Pg} = \frac{\mathrm{Eg} \times 3600}{\Delta t} \quad \text{(S11)}$$

Areal energy and power density in μW h cm^{-2} and mW cm^{-2} respectively

$$\mathrm{EA} = \frac{1 \times C_A \times (\Delta V^2)}{2 \times 3.6} \quad \text{(S12)}$$

$$\mathrm{PA} = \frac{E_A \times 3600}{\Delta t} \quad \text{(S13)}$$

Volumetric energy and power density in W h L^{-1} and W L^{-1} respectively

$$E_V = E_g \text{ x } \rho \quad \text{(S14)}$$

$$P_V = P_g \text{ x } \rho \quad \text{(S15)}$$

Where C_g = gravimetric capacitance in F g^{-1}, C_A = areal capacitance in mF cm^{-2}, C_v = volumetric capacitance in F cm^{-3}, ρ = mass density of the HSC device in g cm^{-3}, I = discharge current in Ampere, m_t = sum of the masses of active materials on both the electrodes in g (m^++m^- for hybrid supercapacitor), A= Area of the active electrode material in cm^2, Δt = discharge time, and ΔV = operating voltage window of HSC device.

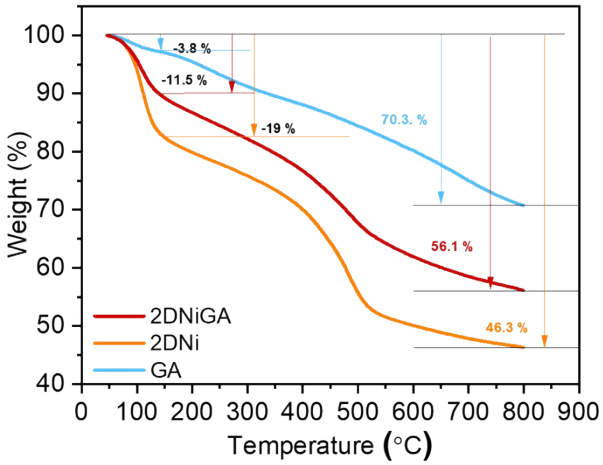

Figure S1. Thermogravimetric analysis (TGA) of GA, 2DNi, and 2DNiGA samples performed under an inert atmosphere. Comments: initial weight losses observed up to 140 °C correspond to the desorption of water and residual solvents. For the 2DNi and 2DNiGA samples, major weight loss occurs from 450 to 550°C, indicative of the MOF structural decomposition. Based on the results and considering the following two equations, the mass of GA (m_{GA}) and the mass of 2DNi (m_{2DNi}) in the 2DNiGA hybrid can be calculated. For the hybrid before combustion, we consider that the masses of the two components are equal to 100 units: $m_{GA}+m_{2DNi} = 100$. From the TGA residual masses of the pristine GA and 2DNi materials, it is obtained that 70.3 % is left from GA and 46.3 % is left from 2DNi. Therefore, for the hybrid after combustion, it is $0.703*m_{GA}+0.463*m_{2DNi} = 56.1$. Solving these two equations, the contents of GA and 2DNiGA in the hybrid are obtained as: m_{GA}=~41 % and m_{2DNi}=~59%.

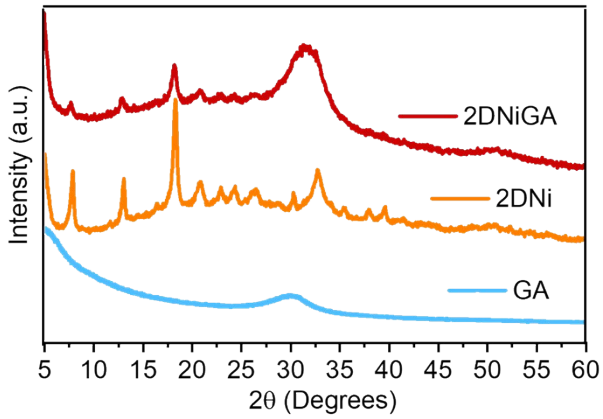

Figure S2. XRD spectra of GA, 2DNi, and 2DNiGA samples.

XRD diffraction patter of the 2DNiGA and 2DNi showed peaks at 2θ = 5.5°, 11.1°, 16.4°, 19.4°, 21.2°, 22.7°, 24.9°, 28.9°, 31.5°, 34.3°, 36.9°, and 38.7° correspond to the (100), (110), (200), (210), (310), (400), (410), (420), (211), (001), (301), and (221) crystal planes, respectively, demonstrating hexagonal packing within the ab planes. [3–6] The peak at 31.5° in 2DNi indexed to the (211) lattice planes is not visible in 2DNiGA due to the presence of a GA peak at 30.5°. According to Debye–Scherrer's formula, as shown in Eq. S1 below

$$D = \frac{k\lambda}{\beta\, Cos\theta} \qquad \text{(S16)}$$

where β represents the FWHM (Full Width at Half Maximum) measured in radians, λ is the wavelength of X-rays, D is the crystallite size, and k is a constant. the average crystallite size of pristine 2DNi is 19.8 nm, whereas the crystallite size in the composite is 17.3 nm. This can be attributed to the introduction of GA, which acts as nucleation sites, leading to the formation of smaller crystallites during the growth process.

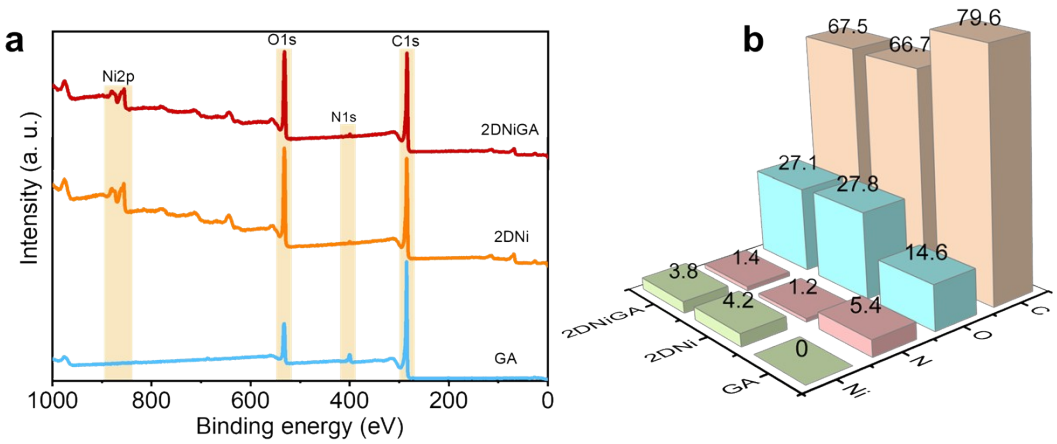

Figure S3. XPS analysis of 2DNiGA, 2DNi, and GA samples: (a) Survey Scan, and (b) Elemental compositions

The small quantity of nitrogen (1.2%) in the MOF sample could be due to the impurities in the precursors, considering that the HHTP and nickel acetate were used without purification, being 95% pure from TCI. Trace amine or nitrate-based impurities could be present in the precursors, especially if the purity is <99%. Over an 18-hour synthesis, even low-level impurities could be incorporated or adsorbed onto the surface. The nitrogen content in the GA (5.4 at. %) is due to its precursor of (cyanographene – G-CN), since GA is produced from the controlled hydrolysis of G-CN.[7] The nitrogen content in the composite is thus mainly due to the GA.

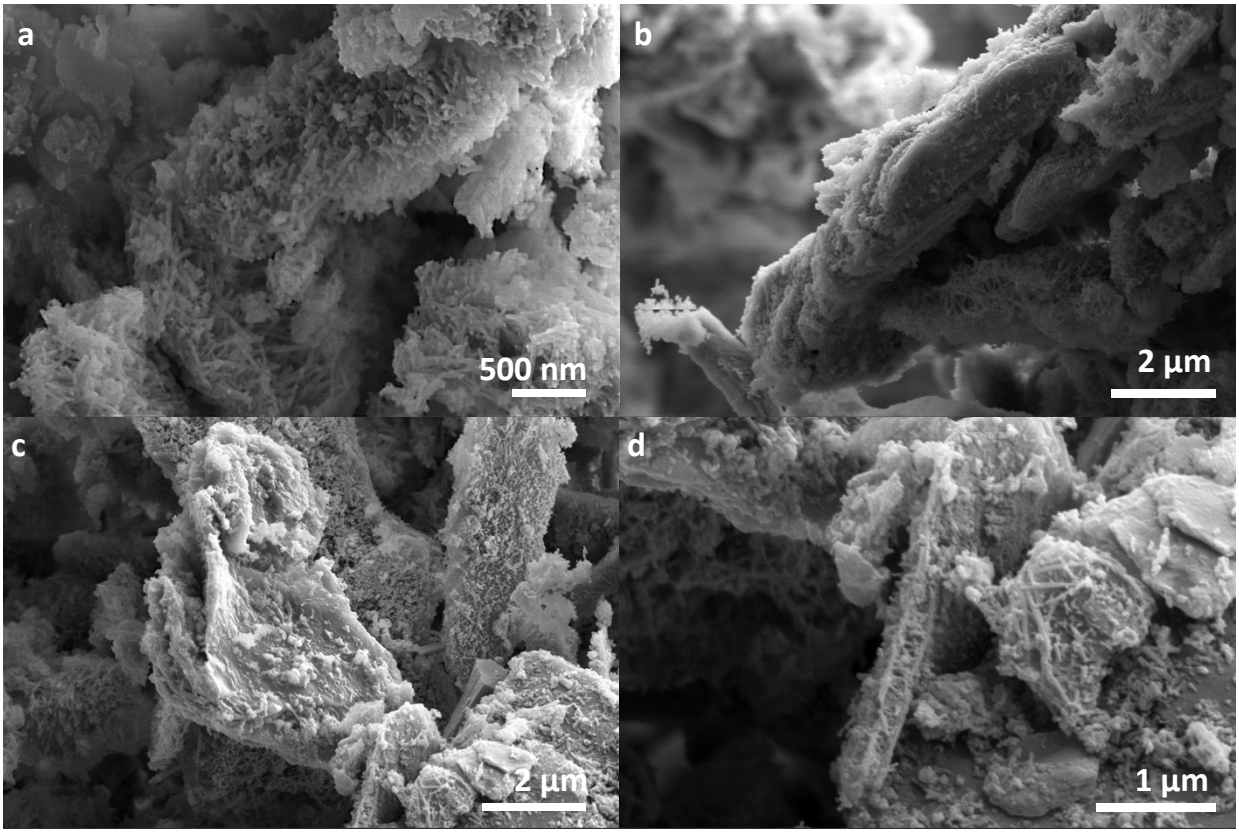

Figure S4. (a-d) Cross-sectional SEM images of the 2DNiGA.

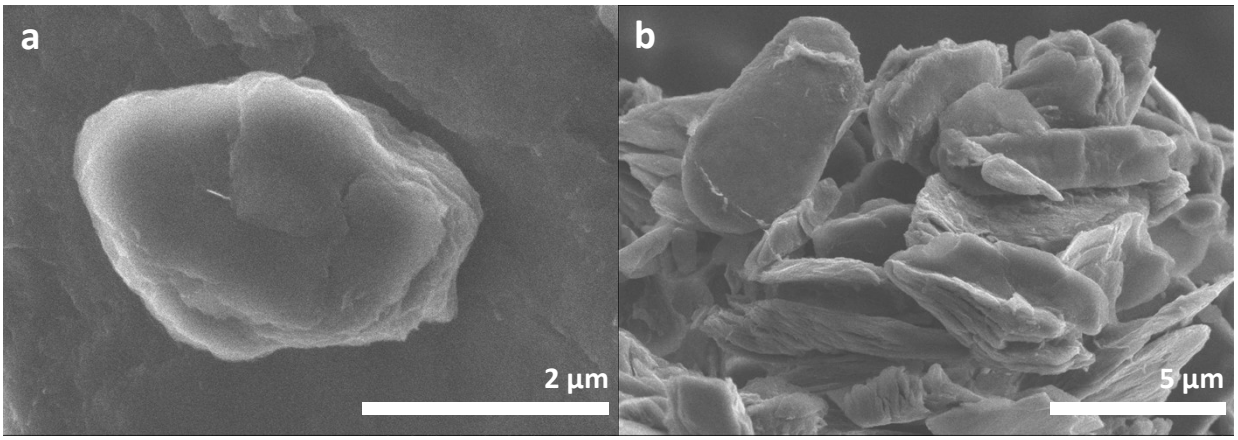

Figure S5. (a,b) SEM images of the GA.

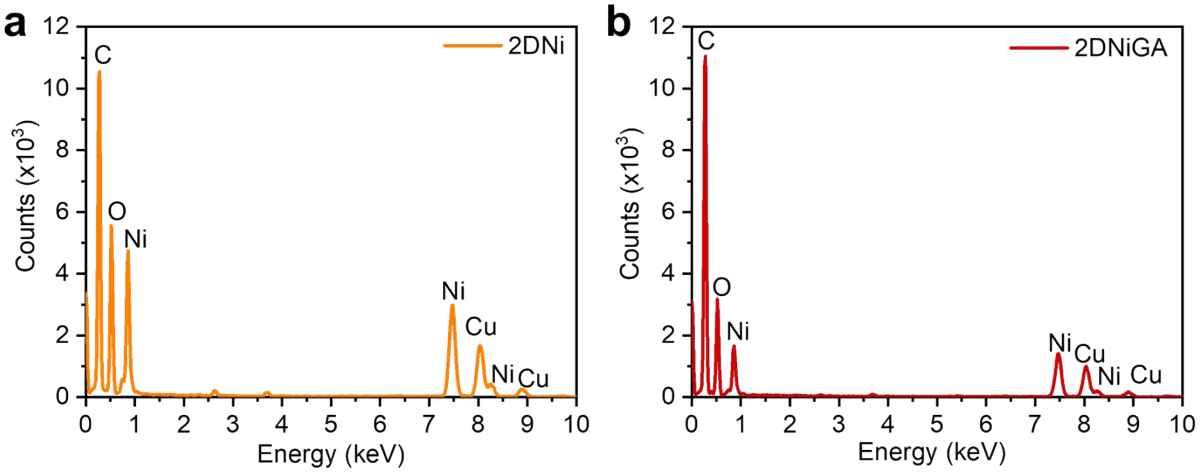

Figure S6. TEM-EDS spectra of (a) 2DNi, and (b) 2DNiGA samples.

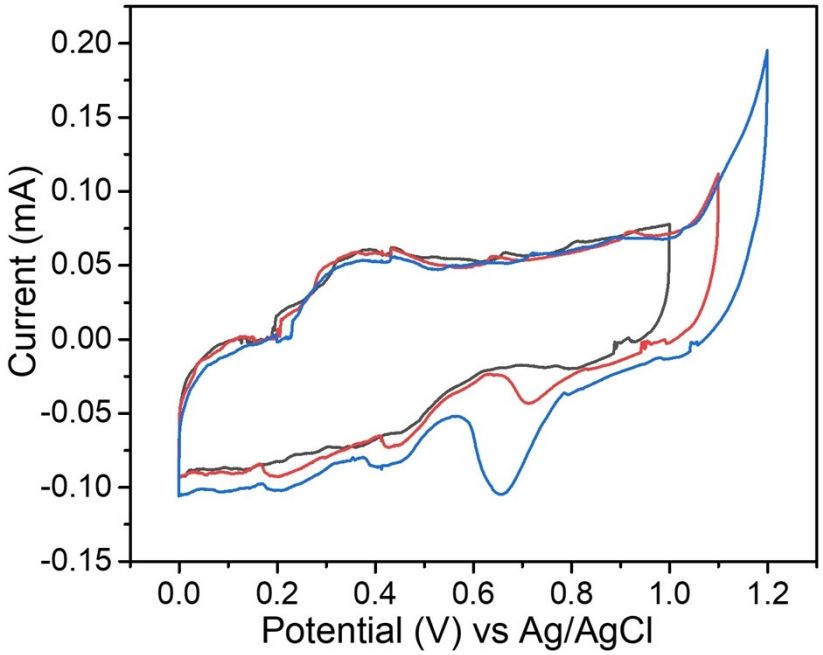

Figure S7. Potential window test for 2DNiGA electrode material in 1M H_2SO_4 at the scan rate of 0.2 mV s^{-1}.

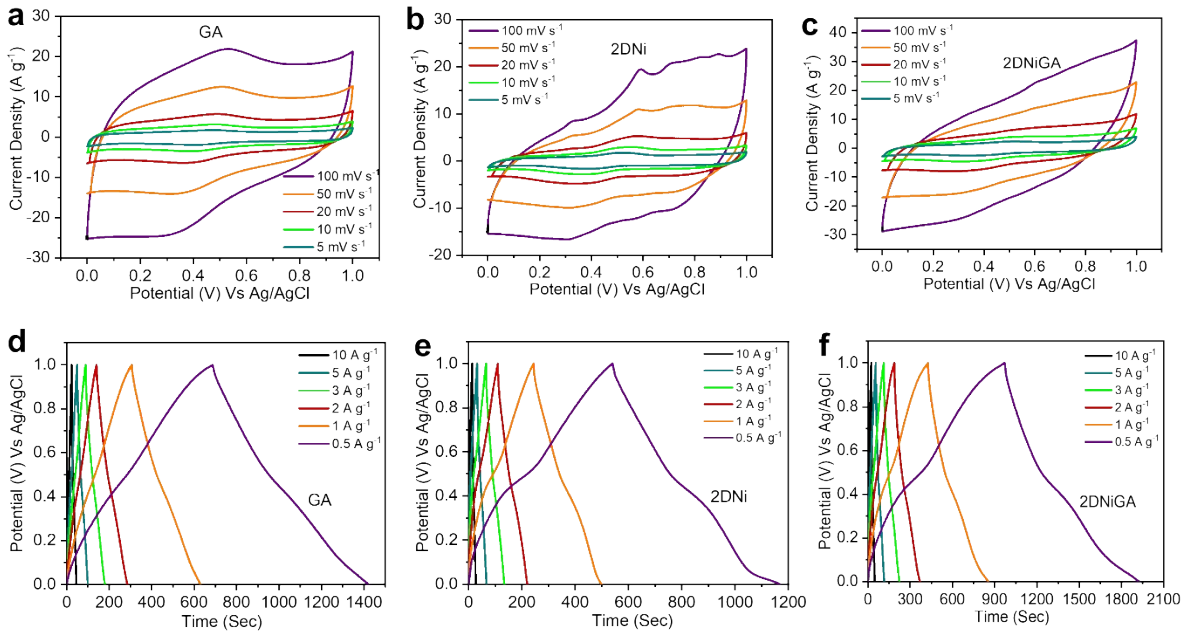

Figure S8. Electrochemical analysis in three electrode system, CV at different scan rates: (a) GA, (b) 2DNi and (c) 2DNiGA, and GCD at different current densities: (d) GA, (e) 2DNi and (f) 2DNiGA.

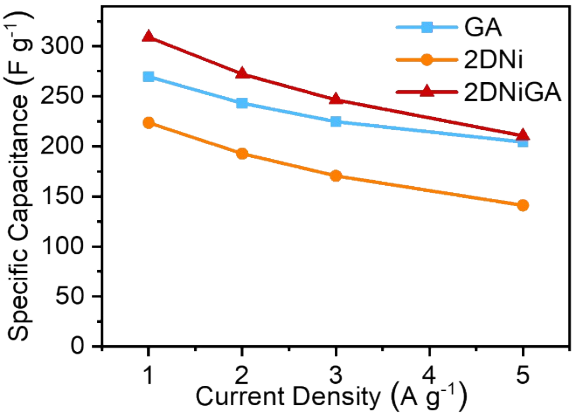

Figure S9. Variation of specific capacitance with respect to current densities for GA, 2DNi, and 2DNiGA.

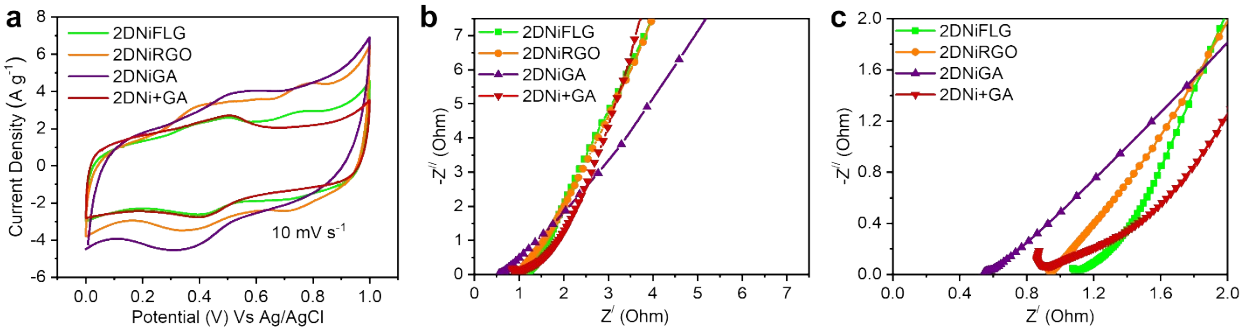

Figure S10. Electrochemical performance comparison of 2DNiFLG, 2DNiRGO, 2DNiGA, and 2DNi+GA electrodes: (a) CV comparison at a constant scan rate of 10 mV s^{-1}, (b) Nyquist plot comparison, and (c) Magnified Nyquist plot comparison.

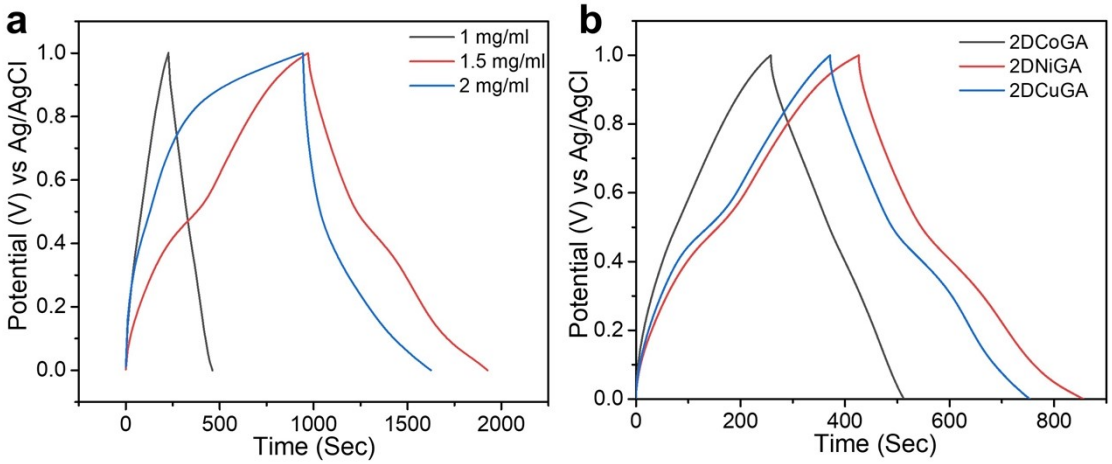

Figure S11. GCD comparison of 2DNiGA composite material with different concentrations of GA (1 mg ml^{-1}, 1.5 mg ml^{-1}, and 2 mg ml^{-1}) used in synthesis, and (b) GCD comparison of other 2D conducting MOF with 2DNiGA.

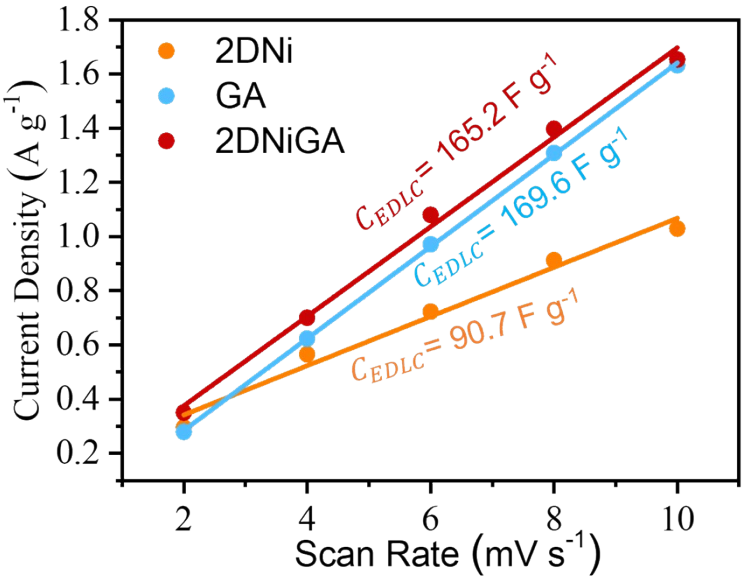

Figure S12. Cathodic current density with respect to scan rate for GA, 2DNi, and 2DNiGA.

,

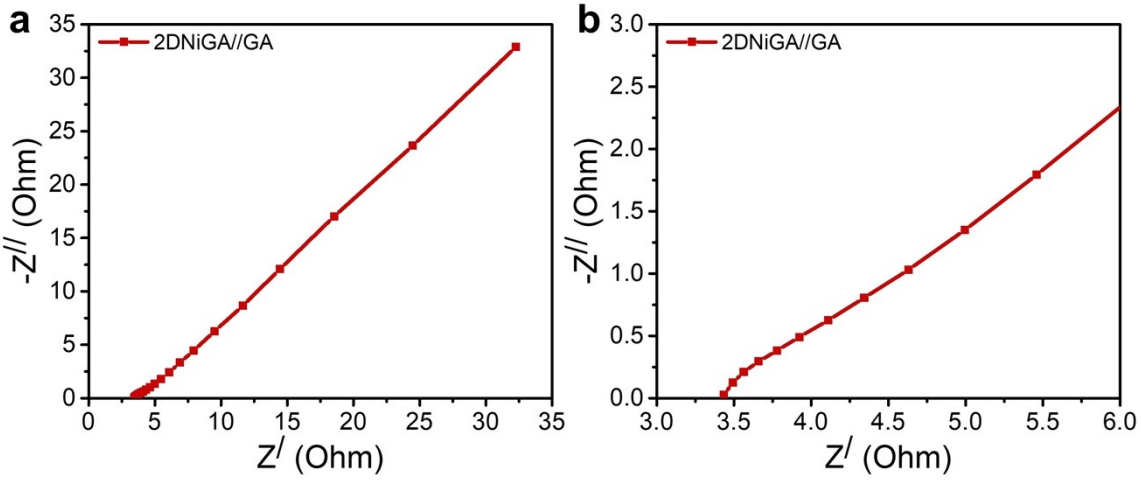

Figure S13. (a) Nyquist plot of 2DNiGA//GA HSC device, and (b) corresponding magnified Nyquist plot.

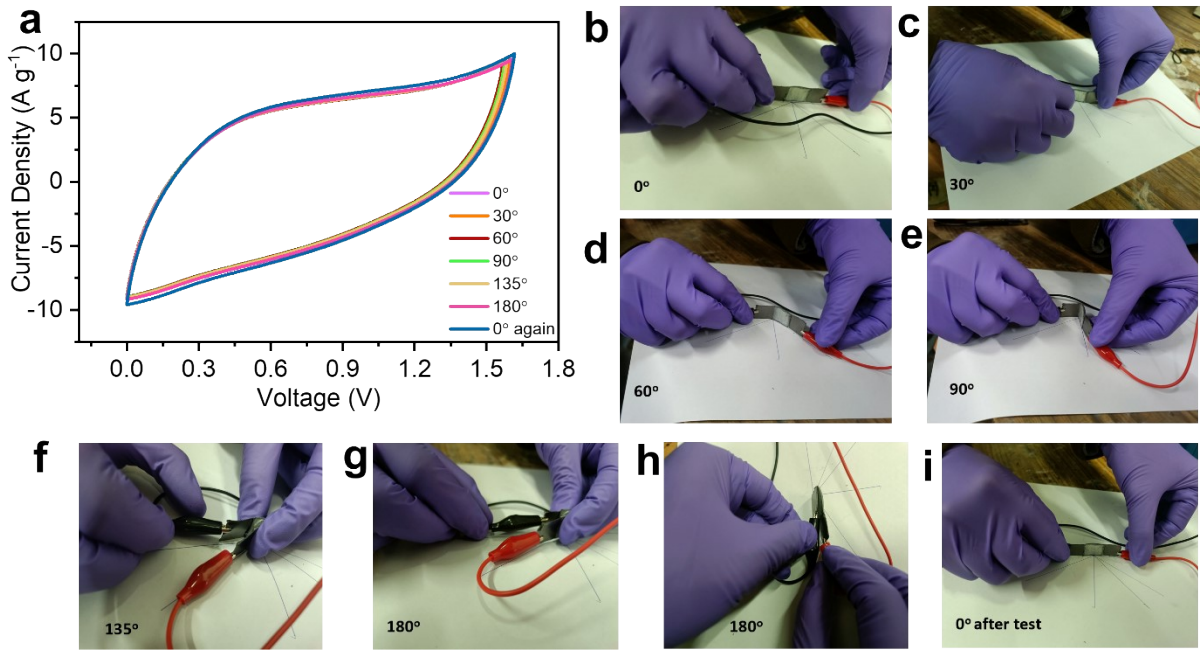

Figure S14. Flexibility test of 2DNiGA//GA 1.6V HSC Device: (a) CV comparison at a scan rate of 50 mV s^{-1}, (b) device at straight condition 0°, (c) bend at 30°, (d) bend at 60°, (e) bend at 90°, (f) bend at 135°, (g) bend at 180° side view, (h) bend at 180° top view, and (i) 0° after test.

Table S1. Electrochemical performance comparison of 2DNiGA composite with other reported electrodes for supercapacitor applications.

#	Electrode Material	**Mass loading** (mg cm^{-2}); **electrolyte; voltage** (V)	C_{sp} (F g^{-1}) @ I_d (A g^{-1}); E_{sp} (Wh kg^{-1})@P_{sp} (W kg^{-1})	C_{sp} **retention @ cycles, cycling rate** (A g^{-1})	**Reference**
1.	Copper-Hexahydroxy triphenylene (Cu-HHTP) MOF (MOF//AC Asymmetric)[a]	4.0; 1M KOH; 0.6 (3-el.) N.A.; 1M KOH, 1.6 (2-el.)	C_{sp}:336.6 @ 1 (3-el.) C_{sp}:86.2@ 1 (2-el) E_{sp}:33 @ 3582	95% @ 1000, N.A.	Mater. Today Sustain. 2023 [8]
2.	2D Cobalt-Catecholate (Co-CAT) MOF	1.0; 1M Na_2SO_4; 1 (3-el.)	C_{sp}: 239 @ 1 (3-el.) N.A. (2-el.)	98.5% @ 10000, 10	Adv. Mater. 2022 [9]
3.	2D Nickel-Catecholate (Ni-CAT) MOF	1.0; 1M Na_2SO_4; 1 (3-el.)	C_{sp}: 233 @ 1 (3-el.) N.A. (2-el.)	97.2% @ 10000, 10	
4.	2D Copper-Catecholate (Cu-CAT) MOF; Symmetric	0.6; 3M KCl; 0.5 (3-el.) 4; PVA-3M KCl; 0.8 (2-el.)	C_{sp}: 202 @ 0.5 (3-el.) C_{sp}: 120 @ 0.5 (2-el.) E_{sp}: 2.6 @ 200	85% @ 5000, 50 mV s^{-1}	Adv. Func. Mat. 2017 [10]
5.	Titanium Carbide	2; 1M KOH; 0.6 (3-el.)	C_{sp}: 130 (442 F cm^{-3})	99% @ 10000,	Science 2013[11]

#	Electrode Material	**Mass loading** (mg cm^{-2}); **electrolyte; voltage** (V)	**C_{sp}** ($F\ g^{-1}$) **@ I_d** ($A\ g^{-1}$); **E_{sp}** ($Wh\ kg^{-1}$)**@P_{sp}** ($W\ kg^{-1}$)	**C_{sp} retention @ cycles, cycling rate** ($A\ g^{-1}$)	**Reference**
	MXene		@ 2 mV s^{-1} (3-el.) N.A. (2-el.) E_{sp}: 5.5 (18.5 W h L^{-1}) @ 70 (0.24 kW L^{-1})	1	
6.	Electrolyte-mediated chemically converted graphene (EM-CCG)	1; 1M H_2SO_4; 1 (3-el.)	C_{sp}: 170.6 (226.9 F cm^{-3}) @ 1 (3-el.) N.A. (2-el.) E_{sp}: 7 @ 250	95% @ 5000, 2.5	Science 2013 [12]
7.	2D Copper-Catecholate/Polypyrrole (Cu-CAT/PPy) Composite, Symmetric	2.01; 3M KCl; 0.5 (3-el.) 4.02; PVA-LiCl; 0.8 (2-el.)	C_{sp}: 463 mF cm^{-2} @ 1.25 mA cm^{-2} (3-el.) C_{sp}: 252.1 mF cm^{-2} @ 1.25 mA cm^{-2} (2-el.) E_{sp}: 22.4 µWh cm^{-2} @ 1.1 mW cm^{-2}	90% @ 8000, 100 mV s^{-1}	Adv. Energy Mater. 2020 [13]
8.	2D Nickel Hexaaminobenzene (Ni-HAB)[b]	9; 1 M KOH; 0.5 (3-el.)	Using GCD C_{sp}: 400 (720 F cm^{-3}) @ 1 (3-el.) E_{sp}: 13.88 (24.98 W h L^{-1})/ 249.84 (0.449 kW L^{-1}) Using CV C_{sp}: 335 (603 F cm^{-3}) @ 5 mV s^{-1} (3-el.) E_{sp}: 11.6 (20.7 W h L^{-1})/ 419 (0.74 KW L^{-1})	90% @ 12000, 10	Nat. Energy. 2018 [14]
9.	Graphene/MnO_2//Densely Stacked Graphene (G/MnO_2//DSG) (Asymmetric) [c]	2; 1 M Na_2SO_4; 1 (3-el.) N.A.; 1 M Na_2SO_4; 1.8 (2-el.)	C_{sp}: 216 @ 0.5 (3-el.) C_{sp}: 72 (62.8 F cm^{-3}) @ 1 (2-el.) E_{sp}: 32.4 (28.2 W h L^{-1}) @ 900 (0.784 kW L^{-1})	90% @ 5000, 200 mV s^{-1}	Small 2016[15]
10	Bismuth-Hexahydroxy triphenylene (Bi-HHTP) MOF ($Ni(OH)_2$//Bi-HHTP Asymmetric)[d]	2.0; 3 M KOH; 1 (3-el.) N.A.; 6 M KOH; 1.5 (2-el.)	C_{sp}: 234 @ 1 (3-el.) C_{sp}: 55 @ 1 (2-el.) E_{sp}: 17.1 @ 746.1	92.5% @1000, 10	Dalton Trans. 2023 [16]
11	Nickel-Hexaimino triphenylene (Ni-HITP) MOF (Symmetric)[e]	5; 1 M $TEABF_4$/ACN; 1 (3-el.) 7; 1 M TEABF4/ACN; 1 (2-el.)	N.A. (3-el.) C_{sp}: 70 (42 F cm^{-3}) @ 1 (2-el.) E_{sp}: 2.43 (14.5 W h L^{-1}) @ 499.8 (0.3 kW L^{-1})	90% @10000, 2	Nat. Mater. 2017 [17]

#	Electrode Material	**Mass loading** (mg cm^{-2}); **electrolyte; voltage** (V)	**C_{sp}** (F g^{-1}) **@ I_d** (A g^{-1}); **E_{sp}** (Wh kg^{-1})**@P_{sp}** (W kg^{-1})	**C_{sp} retention @ cycles, cycling rate** (A g^{-1})	**Reference**
12	Carbon nanotubes/graphene petals (CNT-GP) (Symmetric)	N.A.; 1 M H_2SO_4; 1 (3-el.) N.A., 1 M H_2SO_4; 1 (2-el.)	C_{sp}: 500 @ 1 mA cm^{-2} (3-el.) C_{sp}: 675 mF cm^{-2} @ 3 mA cm^{-2} (2-el.) E_{sp}: 16 (4 W h L^{-1}) @ 200 (0.0065 kW L^{-1})	91% @ 20000, 80 mA cm^{-2}	Nat. Commun. 2018 [18]
13	MOF-derived graphene nanoribbons (GNRib) (Symmetric)[f]	N.A. (3-el.) 4; 1 M H_2SO_4; 1 (2-el.)	N.A. (3-el.) C_{sp}: 168 @ 1 (2-el.) E_{sp}: 5.8 @ 250	95% @ 500, 10 mV s^{-1}	Nat. Chem. 2016 [19]
14	Oriented MOF on carbon fiber paper (MOF/CFP) (Asymmetric)	2 ;1 M KOH; 0.45 (3-el.) 5; 1 M KOH; 1.5 (2-el.)	C_{sp}: 1044 @ 2 (3-el.) C_{sp}: 92.66 @ 1 (2-el.) E_{sp}: 28.5 @ 1500	94% @ 5000, NA	Adv. Energy Mater. 2018 [20]
15	h-MoO_3//CuCoHCF (h-MoO_3) (Asymmetric)[g]	1; 0.5 M H_2SO_4; 0.53 (3-el.) 2.2; 0.5 M H_2SO_4; 1.6 (2-el.)	C_{sp}: 547 @ 1 (3-el.) C_{sp}: 80.3 @ 1 (2-el.) E_{sp}: 27.8 @ 789.1	83 % @ 10000, 10	Nature. Commun. 2023[21]
16	Graphene-Embedded Cyclodextrin-Metal-Organic Framework (γ-CD-MOF/GO/MG-600) (Symmetric)	N.A. ;1 M H_2SO_4; 1 (3-el.) N.A.; 1 M H_2SO_4; 1.4 (2-el.)	C_{sp}: 501 @ 0.5 (3-el.) C_{sp}: 111.3 @ 1 (2-el.) E_{sp}: 30.3 @ 700	90.1% @ 5000, 5	Adv. Sci. 2023[22]
17	Cu_3-(HHTATP)$_2$ (HHTATP: 2,3,6,7,10,11-hexahydroxy-1,5,9-triaminotriphenylene)	15-17;1 M KCl;0.9 (3-el.) 30-34;1 M KCl;1 (2-el.)	C_{sp}: 340 @ 0.2 (3-el.) C_{sp}: 66 @ 0.5 (2-el.) E_{sp}: 9.33 @ 250	94% @ 7000, 5	J. Am. Chem. Soc. 2024[23]
2DNiGA//GA HSC		**1; 1 M H_2SO_4; 1 (3-el.), ρ=0.833 g cm^{-3}** **3; 1 M H_2SO_4; 1.6(2-el.), ρ=1.04 g cm^{-3}**	**C_{sp}: 309 @ 1 (3-el.)** **C_{sp}: 200 @ 1 (2-el.)** E_{sp}: **71 @ 800** **309 mF cm^{-2} @ 1 mA cm^{-2} (3-el.)** **600 mF cm^{-2} @ 3 mA cm^{-2} (2-el.)** **213 µWh cm^{-2}/2.4 mW cm^{-2}** **257.4 F cm^{-3} @ 1 mA cm^{-2} (3-el.)** **208 F cm^{-3} @ 3 mA cm^{-2} (2-el.)** **73.8 W h L^{-1} /0.836 kW L^{-1}**	**96.1 % @ 10000, 10**	**This work**

[a] This paper reports specific capacity in C g^{-1} for both three and two-electrode systems, therefore to calculate specific capacitance in F g^{-1}, the specific capacity is divided by the potential for both three-electrode (0.6V) and two-electrode (1.6 V) system.
[b] This paper reports specific capacitance, energy and power density using CV data only. However, in Fig.31 of supplementary information, GCD curves are given, therefore gravimetric and volumetric specific capacitance, energy, and power density have been calculated from this GCD curve at 1 A g^{-1}.

[c] The energy and power density reported at very low current density of 0.1 A g^{-1}, therefore the energy and power density were recalculated at a current density of 1 A g^{-1}. All the calculations were based on Figure S11.

[d] The Cs =55 F g^{-1} at 1 A g^{-1} is given for ASC device but energy and power density are not given, so Energy and Power density for ASC is recalculated to be 17.1 W h Kg^{-1} and 746.1 W kg^{-1}.

[e] The Cs= 70 F g^{-1} at 1 A g^{-1} is given for symmetrical supercapacitor, energy, and power density is not given, so Energy and Power density for symmetrical SC is recalculated to be 2.43 W h Kg^{-1} and 499.8 W kg^{-1}.

[f] The Cs= 168 F g^{-1} at 1 A g^{-1} is given for symmetrical supercapacitor, energy, and power density are not given, so Energy and Power density for symmetrical SC is recalculated to be 5.8 W h Kg^{-1} and 250 W kg^{-1}.

[g] The specific capacitance in both three and two-electrode systems is given only from CV, therefore it has to be recalculated from GCD curves. Based on the GCD values, the energy and power density are again recalculated for asymmetric supercapacitor devices.

References

1 A. Bakandritsos, M. Pykal, P. Błoński, P. Jakubec, D. D. Chronopoulos, K. Poláková, V. Georgakilas, K. Čépe, O. Tomanec, V. Ranc, A. B. Bourlinos, R. Zbořil and M. Otyepka, *ACS Nano*, 2017, **11**, 2982–2991.
2 M. Hmadeh, Z. Lu, Z. Liu, F. Gándara, H. Furukawa, S. Wan, V. Augustyn, R. Chang, L. Liao, F. Zhou, E. Perre, V. Ozolins, K. Suenaga, X. Duan, B. Dunn, Y. Yamamto, O. Terasaki and O. M. Yaghi, *Chem. Mater.*, 2012, **24**, 3511–3513.
3 Y.-X. Shi, Y. Wu, S.-Q. Wang, Y.-Y. Zhao, T. Li, X.-Q. Yang and T. Zhang, *J. Am. Chem. Soc.*, 2021, **143**, 4017–4023.
4 B. Hoppe, K. D. J. Hindricks, D. P. Warwas, H. A. Schulze, A. Mohmeyer, T. J. Pinkvos, S. Zailskas, M. R. Krey, C. Belke, S. König, M. Fröba, R. J. Haug and P. Behrens, *CrystEngComm*, 2018, **20**, 6458–6471.
5 J. Liu, Z. Chen, H. Liu, S. Qin, M. Li, L. Shi, C. Zhou, T. Liao, C. Li, Q. Lv, M. Liu, M. Zou, Y. Deng, Z. Wang and L. Wang, *Small*, 2024, **20**, 2305076.
6 C. Guo, Z. Li, F. Duan, Z. Zhang, F. Marchetti and M. Du, *J. Mater. Chem. B*, 2020, **8**, 9951–9960.

7 A. Bakandritsos, M. Pykal, P. Błoński, P. Jakubec, D. D. Chronopoulos, K. Poláková, V. Georgakilas, K. Čépe, O. Tomanec, V. Ranc, A. B. Bourlinos, R. Zbořil and M. Otyepka, *ACS Nano*, 2017, **11**, 2982–2991.
8 M. Shaheen, M. Z. Iqbal, S. Siddique, S. Aftab and S. M. Wabaidur, *Mater. Today Sustain.*, 2023, **23**, 100415.
9 S. Cheng, W. Gao, Z. Cao, Y. Yang, E. Xie and J. Fu, *Adv. Mater.*, 2022, **34**, 2109870.
10 W. Li, K. Ding, H. Tian, M. Yao, B. Nath, W. Deng, Y. Wang and G. Xu, *Adv. Funct. Mater.*, 2017, **27**, 1702067.
11 M. R. Lukatskaya, O. Mashtalir, C. E. Ren, Y. Dall'Agnese, P. Rozier, P. L. Taberna, M. Naguib, P. Simon, M. W. Barsoum and Y. Gogotsi, *Science*, 2013, **341**, 1502–1505.
12 X. Yang, C. Cheng, Y. Wang, L. Qiu and D. Li, *Science*, 2013, **341**, 534–537.
13 R. Hou, M. Miao, Q. Wang, T. Yue, H. Liu, H. S. Park, K. Qi and B. Y. Xia, *Adv. Energy Mater.*, 2020, **10**, 1901892.
14 D. Feng, T. Lei, M. R. Lukatskaya, J. Park, Z. Huang, M. Lee, L. Shaw, S. Chen, A. A. Yakovenko, A. Kulkarni, J. Xiao, K. Fredrickson, J. B. Tok, X. Zou, Y. Cui and Z. Bao, *Nat. Energy*, 2018, **3**, 30–36.
15 L. Sheng, L. Jiang, T. Wei and Z. Fan, *Small*, 2016, **12**, 5217–5227.
16 S. Chen, H. Zhang, X. Li, Y. Liu, M. Zhang, X. Gao, X. Chang, X. Pu and C. He, *Dalton Trans.*, 2023, **52**, 4826–4834.
17 D. Sheberla, J. C. Bachman, J. S. Elias, C.-J. Sun, Y. Shao-Horn and M. Dincă, *Nat. Mater.*, 2017, **16**, 220–224.
18 G. Xiong, P. He, Z. Lyu, T. Chen, B. Huang, L. Chen and T. S. Fisher, *Nat. Commun.*, 2018, **9**, 790.
19 P. Pachfule, D. Shinde, M. Majumder and Q. Xu, *Nat. Chem.*, 2016, **8**, 718–724.
20 T. Deng, Y. Lu, W. Zhang, M. Sui, X. Shi, D. Wang and W. Zheng, *Adv. Energy Mater.*, 2018, **8**, 1702294.
21 T. Xu, Z. Xu, T. Yao, M. Zhang, D. Chen, X. Zhang and L. Shen, *Nat. Commun.*, 2023, **14**, 8360.
22 W. Zhang, Z. Zheng, L. Lin, X. Zhang, M. Bae, J. Lee, J. Xie, G. Diao, H. Im, Y. Piao and H. Pang, *Adv. Sci.*, 2023, **10**, 2304062.
23 G. Lee, G. Park and S. S. Park, *J. Am. Chem. Soc.*, 2024, **146**, 29767–29772.